Time-lapse seismic changes in a CO_2 injection process in a fractured reservoir

Erika Angerer, Stuart Crampin, University of Edinburgh*
Xiang-Yang Li, British Geological Survey
Thomas L. Davis, Colorado School of Mines

Summary

The time delay changes of stacked time-lapse shear-wave data show a significant 10% change in anisotropy before and after a CO_2 injection process in a fractured dolomite reservoir in Vacuum Field, New Mexico. The time-lapse *P*-wave data do not show comparable variations in interval travel times. A combined model based on the anisotropic poro-elasticity theory, APE, (Zatsepin and Crampin, 1997) and on Kuster-Tokszos modelling matches the stacked data. Both the saturation change and the measured pore-fluid pressure increase of 1000 psi are considered. The model explains these observations as a pressure effect with the dynamic opening and closing of near-vertical low aspect ratio pores to which shear-wave splitting is more sensitive than *P*-wave velocities.

Introduction

Time-lapse seismic is successfully used in many unconsolidated and soft rock reservoirs (Jack, 1998). However, for hard rocks like carbonates and consolidated sandstones, it is less likely to detect saturation changes due to their higher stiffness. The detectability of pressure changes in such rocks largely depends on the presence of fractures as observed in laboratory experiments by Hirsche et al. (1997).

In a fractured dolomite reservoir in Vacuum Field, New Mexico, in a tertiary recovery process, CO_2 was injected in a single well over a period of three weeks and two 3D 9C seismic surveys were acquired immediately before and after the injection. Sources and 3C receivers were positioned at the same locations for both surveys to ensure high repeatability in the acquisition. A pore-fluid pressure increase of 1000 psi was recorded (Roche et al. 1997). Here we perform shear-wave splitting and *P*-wave interval time analysis on this time-lapse dataset to quantify any changes in anisotropy and to model and explain such changes using inclusion based anisotropic theories.

Data processing and analysis

Mainly surface-consistent algorithms are used during processing to improve repeatability. To ensure that the anisotropic information (time delays and polarisation directions) is preserved during processing, some critical processing steps (deconvolution, dip-filter, f-x deconvolution, stacking) are tested on full-wave synthetic data before applied to real data. For each multicomponent dataset one P-wave and four shear-wave volumes are produced. The processing, partly performed by Roche (1997), consists of the following steps for the shear-waves: vibroseis crosscorrelation, trace edit, refraction statics, Alford rotation to the natural co-ordinate system (118°-28°), surface-consistent deconvoluiton, phase matching, mute, NMO correction, reflection statics, stack, 3D f-x deconvolution, dip-filter, and gain.

Within each survey all shear-wave datasets have the same statics applied, and one 3D velocity function is used in both surveys. Also one gain function function is derived and applied to all shear-wave data sets. The P-wave processing flow consists of the same steps as the one for shear excluding the rotation.

Anisotropic analysis is performed on stacked data. Horizon tracking provides interval travel times and time-delays of the split shear waves, which are used to calculate the percentage shear-wave anisotropy as the normalised difference between the fast and the slow shear-wave velocities. P-wave time delays (horizon mis-ties) before and after injection are also calculated for comparison. The injection interval comprises about 200 ms in shear and 100 ms in *P*. Figure 1 shows the interval time analysis results before and after injection for shear and the interval time difference for *P*. Figure 1a and 1b are the percentage time delays between the fast and the slow shear-waves of the two surveys and 1c shows the percentage difference in shear-wave anisotropy before and after injection. Figure 1d is the interval time difference plot for the P-waves. The picking error is ±2%, which makes only significant changes detectable. Before the injection, the shear-wave time delays lie between ±2%, which means shear-wave splitting is low.

After the injection a zone with negative shear-wave splitting can be observed in Figure 1b to the south and east of the injection well. Negative anisotropy means that the shear-wave polarised parallel to the maximum horizontal stress direction is slower than the perpendicularly polarised wave. A similar observation of a negative anisotropy or a 90° polarisation change in an over-pressurised reservoir was made by Crampin et al. (1996). The shear-wave difference plot, 1c, shows that the injection caused a clear increase in anisotropy. The P-wave time delay difference plot, Figure 1b, does not show any changes that are outside

the range of the picking error. Analysis of reflections above the target interval shows that the shear-wave velocities in the overburden are also affected by the injection with an increase in velocity of up to 2%.

Polarisation analysis was performed using the linear transform technique (Li and Crampin, 1993). In the overburden, the polarisation directions lie around 118° NE, the maximum horizontal stress direction. In the target, the polarisations are heterogeneous before injection and become less variable after the injection related pore-fluid pressure increase.

Interpretation and modelling

A location close to the injection well was chosen for 1D full waveform anisotropic modelling of the flat layered, structurally simple evaporite and dolomite sequence. The layer thicknesses are derived from logs and interval velocities from VSP data and the picked velocity function. The time lapse modelling of the target formation, a fractured dolomite with average porosity of 12.8 %, consists of two parts. The pore space consists of stiff high aspect ratio pores, and compliant low aspect ratio pores making up less than 0.1% of the total porosity. The effect of the saturation change in the stiff cracks is considered in a model (Endres and Knight, 1998), which is inclusion based using the Kuster-Toksöz theory and allows to be calculated the elastic constants at the low frequency limit. In the case of CO_2 injection, which is liquid at the given pressures, the shear-wave velocity is unaffected by the saturation change and the *P*-wave velocity decreases only about 1.5% due to the high stiffness of the rock.

The effect of the pore-fluid pressure increase on low aspect ratio cracks can be modelled with APE. Shear-wave coherency analysis suggests the presence of two fault zones to the south of the well with fault orientations of N and ENE. Cracks were introduced in the following way: there are two cracks sets with 5% crack density each centred around N and ENE and 5% randomly orientated cracks. A 2D simplification of the evolution of this heavily fractured rock mass under increasing pore-fluid pressure is shown in Figure 2. As the overburden pressure is the largest stress, all open cracks are vertical or close to vertical. The direction of maximum horizontal stress is 118° NE, and before injection only cracks close to this direction are open. When the pore-fluid pressure increases 1000 psi, additional cracks open up; especially the fault-related cracks although these are oblique to the maximum horizontal stress.The fit of the synthetic seismograms to the shear-wave and *P*-wave data is shown in Figure 3. In the target zone between 1.6 and 1.8 s the synthetic and the data match very well. In *P* the target interval lies between 0.7 and 0.8 s. In the model all body wave velocities decrease, but most significantly the shear-wave parallel to the maximum horizontal stress and therefore observable changes in anisotropy result. The opening cracks are mostly close to vertical and only affect the *P*-waves at higher angles of incidence. The current model confirms that at normal incidence the combined effects of saturation and pressure change are not strong enough to be detected in the *P*-wave stacks.

Conclusions

In the heavily fractured zone to the south of the CO_2 injection well the pore-fluid pressure increase causes a significant differential change in the shear-wave velocities because of the opening up of cracks. Due to the mainly vertical direction of the open cracks the shear-waves are more sensitive to the pressure changes than the *P*-waves. The saturation change itself cannot be detected due to the high stiffness of the rock matrix. In the case of significant pore-fluid pressure changes in fractured rocks, shear-waves may prove to be very useful in the monitoring of subsurface pressure changes in reservoirs.

Acknowledgement

Erika Angerer wishes to thank Western Geophysical for the financial support of the project and the Reservoir Characterization Project of Colorado School of Mines for providing the seismic data.

References

Jack, I., 1998. Time-Lapse Seismic in Reservoir Management. 1998 SEG Distinguished Instructor Short Course.

Crampin, S., Zatsepin, S.V., Slater, C., and Brodov, L.Y., 1996. Abnormal shear-wave polarizations as indicators of pressure and over pressure, 58th EAGE Conf., Amsterdam, Extended Abstracts, X038.

Endres, A.L., and Knight, R.J., 1997. Incorporating pore geometry and fluid pressure communication into modelling the behavior of elastic rocks. Geophysics, **62**, 106-117.

Hirsche, K., Batzle, M., Knight, R., Wang, Z., Mewhort, L., Davis, R. and Sedgwick, G., 1997, Seismic monitoring of gas floods in carbonate reservoirs: From rock physics to field-testing: 67th Annual Internat. Mtg., Soc. Expl. Geophys., Expanded Abstracts, 902-905 .

Li, X.-Y., and Crampin, S., 1993. Linear transform techniques for processing shear-wave anisotropy in four-component data. Geophysics, **58**, 240-256.

Roche, S.L., Davis, T.L., and Benson, R.D., 1997. 4-D, 3-C seismic study at Vacuum Field, New Mexico, SEG Expanded Abstracts, 886-889.

Zatsepin, S.V. and Crampin, S., 1997. Modelling the compliance of crustal rock – I. Response of shear-wave splitting to differential stress. Geophys. J. Int., **129**, 477-494.

a)

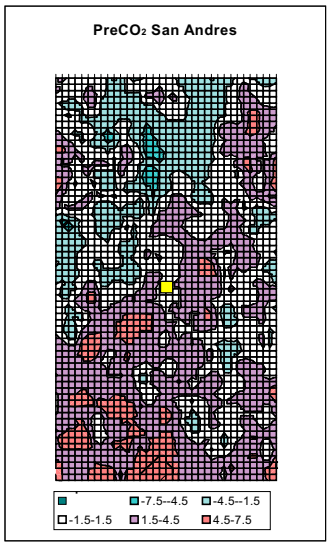

b)

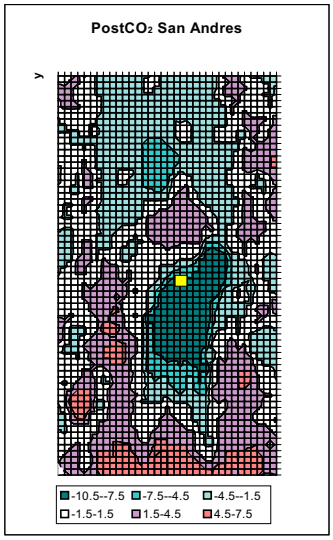

c)

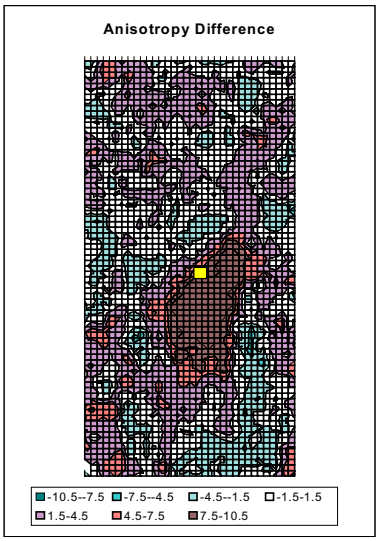

d)

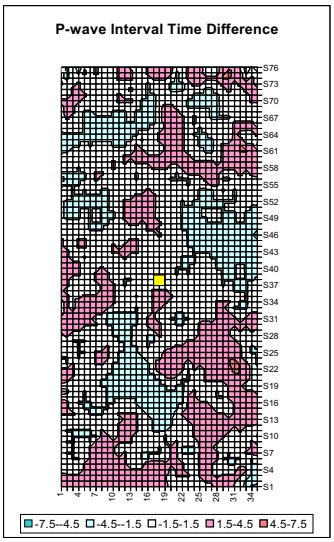

Figure 1: Percent time delays for shear-waves a) before injection, b) after injection; Shear-wave time delay difference, before – after, d) *P*-wave interval time difference, before – after.

a)

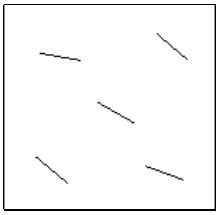

b)

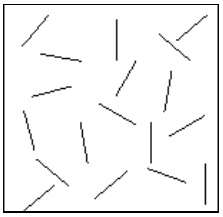

Figure 2: Evolution of crack distribution a) before and b) after pore-fluid pressure increase

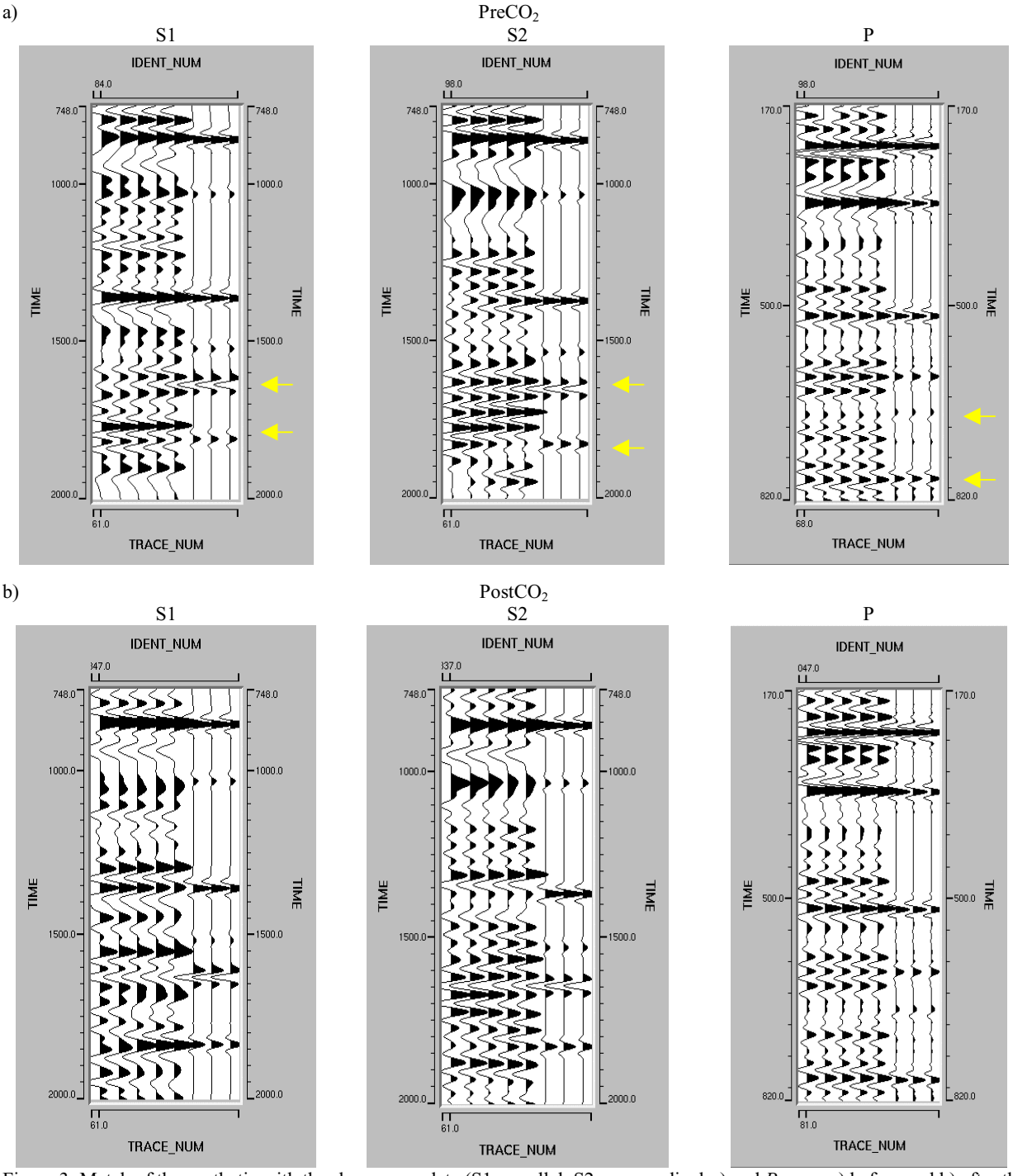

Figure 3: Match of the synthetic with the shear-wave data (S1- parallel, S2 - perpendicular) and *P*-wave a) before and b) after the injection